



**HAL**  
open science

# Ignition of CH<sub>4</sub>:O<sub>2</sub>:Ar and n-C<sub>4</sub>H<sub>10</sub>:O<sub>2</sub>:Ar(N<sub>2</sub>) mixtures with initial temperatures between 650-950 K by a surface pulsed discharge

S.A. Stepanyan, M.A. Boumehdi, G. Vanhove, Pascale Desgroux, Svetlana Starikovskaia, N.A. Popov

## ► To cite this version:

S.A. Stepanyan, M.A. Boumehdi, G. Vanhove, Pascale Desgroux, Svetlana Starikovskaia, et al.. Ignition of CH<sub>4</sub>:O<sub>2</sub>:Ar and n-C<sub>4</sub>H<sub>10</sub>:O<sub>2</sub>:Ar(N<sub>2</sub>) mixtures with initial temperatures between 650-950 K by a surface pulsed discharge. AIAA Aerospace Sciences Meeting, Jan 2014, National Harbor, Maine, United States. 10.2514/6.2014-0665 . hal-02588022

**HAL Id: hal-02588022**

**<https://hal.science/hal-02588022>**

Submitted on 14 Sep 2020

**HAL** is a multi-disciplinary open access archive for the deposit and dissemination of scientific research documents, whether they are published or not. The documents may come from teaching and research institutions in France or abroad, or from public or private research centers.

L'archive ouverte pluridisciplinaire **HAL**, est destinée au dépôt et à la diffusion de documents scientifiques de niveau recherche, publiés ou non, émanant des établissements d'enseignement et de recherche français ou étrangers, des laboratoires publics ou privés.

# Ignition of $\text{CH}_4:\text{O}_2:\text{Ar}$ and $\text{n-C}_4\text{H}_{10}:\text{O}_2:\text{Ar}(\text{N}_2)$ mixtures with initial temperatures between 650-950 K by a surface pulsed discharge.

S. A. Stepanyan\*

*Laboratory of Plasma Physics (CNRS, Ecole Polytechnique, Sorbonne Universities,  
University of Pierre and Marie Curie-Paris 6, University Paris-Sud),  
Route de Saclay, 91128, Palaiseau Cedex, France*

M. A. Boumeهدي† G. Vanhove ‡ and P. Desgroux §

*PC2A Lille University of Science and Technology, 59655, Villeneuve d'Ascq, France*

S. M. Starikovskaia ¶

*Laboratory of Plasma Physics (CNRS, Ecole Polytechnique, Sorbonne Universities,  
University of Pierre and Marie Curie-Paris 6, University Paris-Sud),  
Route de Saclay, 91128, Palaiseau Cedex, France*

N. A. Popov ||

*Skobeltsyn Institute of Nuclear Physics, Moscow State University, Moscow, 119991, Russia*

## I. introduction

Plasma assisted ignition/combustion (PAI/PAC) is a promising application of low temperature plasmas, demonstrating both high industrial abilities and serious non-solved fundamental problems. Modern gas turbine engines operate at high pressure conditions. When plasma ignition starts from low temperatures, two processes are considered to be the most important: first, production of radicals by an electron impact, and second, heating of a gas due to relaxation of electronically excited states (so-called fast gas heating). The length of chemical chains initiated by radicals increases with increase of a gas temperature, and so, the ignition occurs. The detailed kinetics mechanism and role of different components in PAI/PAC chemistry at different  $E/N$  values is still a question of discussion, even for the simplest combustion systems. Recently, different approaches are used to describe the discharge kinetics in PAI/PAC problems. The present work analyses different approaches, from O-atoms addition to detailed kinetics coupled with combustion scheme, and presents the results of numerical calculations for early afterglow of the discharge.

## II. Experimental setup

Experiments on plasma assisted ignition were performed on rapid compression machine (RCM) in PC2 laboratory of Lille University. All the experiments were performed in single pulse mode. Methane/oxygen and

---

\*PhD student, Laboratory for Plasma Physics, Ecole Polytechnique, Palaiseau, France

†PhD Student, Laboratory of Physics of Physico-Chemical Processes in Combustion and in Atmosphere, Lille University, France

‡Senior Researcher, Laboratory of Physics of Physico-Chemical Processes in Combustion and in Atmosphere, Lille University, France

§Leading Researcher, Laboratory of Physics of Physico-Chemical Processes in Combustion and in Atmosphere, Lille University, France

¶Leading Researcher, Laboratory for Plasma Physics, Ecole Polytechnique, Palaiseau, France

||Leading Researcher, Skobeltsyn Institute of Nuclear Physics, Moscow State University, Russia

butane/oxygen mixtures diluted by 76 percent of argon and nitrogen were used in experiments in temperature and pressure ranges presented in Fig. 1. It should be noted that the conditions when autougnition was not possible were investigated for plasma-assisted ignition (see Fig 1).

Fig. 2a schematically represents the combustion chamber of rapid compression machine. The electrode system of the surface dielectric barrier discharge<sup>1</sup> was mounted instead of the endplate of the chamber. The discharge was initiated at the moment of maximal compression when the distance between the piston and the electrode surface is 15 mm.

The characteristic pulse applied to the electrode system to initiate the discharge (Fig. 2b) had the following parameters: amplitude  $\pm(24-55)$  kV, 20 ns duration, 1 ns front rise time. The discharge at these conditions initiates near the edge of the HV electrode (orange color in Fig. 2a) and propagates over the dielectric surface (green color in Fig. 2a) in radial direction to the end of grounded electrode (grey color in Fig. 2a).

At the conditions described above the ignition occurs on the surface of electrode system with further propagation of flame in the chamber. The fast CMOS camera was installed in front of the optical window mounted in combustion chamber to visualize the flame propagation from electrode system to the piston. The length of cylindrical combustion chamber of RCM is 16 mm whereas the diameter of the window is 15 mm, which means that the window covers almost the whole length of the chamber except one millimeter near the end plate where the discharge electrode system is installed. The data obtained with the camera are in agreement with the data obtained with pressure indicator, i.e. sharp rise of pressure corresponds to the consequent ignition of fuel in combustion chamber by coming wave of flame.

The actual induction time was estimated with photomultiplier tube (PMT) installed in front of the optical window instead of the camera. The radiation collected by PMT includes the radiation from the region at less than 1 mm apart the discharge where the ignition occurs. This system allows to establish the upper estimate of the induction time since the sharp rise of voltage at PMT will occur at the moment when after the ignition process the wave of flame reaches the region which covered by PMT and situated at less than 1 mm apart the ignition region.

This work represents only a certain part of the experimental results obtained before, more detailed description of the experiments and obtained results can be found elsewhere<sup>2,3</sup>.

### III. Definitions

For the rest of this paper under efficient induction time we will understand the period between the discharge initiation and the sharp rise of pressure in combustion chamber due to propagation of flame from the discharge, where ignition occurs, to the chamber. This value can be measured by pressure indicator mounted in the chamber.

Under the actual induction time we will understand the period between the discharge initiation and the ignition of the gas mixture in the discharge on the electrode surface. The upper estimation of this value can be made with the data obtained with the photomultiplier as it was described in the end of previous section.

### IV. Experimental results and numerical modeling

The main aim of this paper is numerical analysis of chemical transformations in combustible mixture in the early afterglow of the discharge and the validation of the model on the basis of the experimental data. Using the experimental data obtained at conditions described in previous section (more details can be found in recent publication<sup>2</sup>) one can estimate the energy deposited in the discharge. Fig. 3 demonstrates the dependence of the efficient induction time *vs* applied voltage for the lean methane mixtures diluted by argon. The numbers near the experimental points note the energy absorbed by discharge for different applied voltages. It is seen from the figure that when the discharge energy absorption is below a certain value the efficient induction time is equal to one that occurs in autoignition case. That means that in this case the ignition in the discharge doesn't occur which was verified by the visualization of the ignition process with fast CMOS camera. When a certain value of the integral energy absorption is reached the efficient induction time drops significantly due to the ignition of gas mixture in the discharge and further flame propagation. The values of the deposited energy when the efficient induction time sharply decreases were used as the references for further numerical modeling, i.e. values when the influence of the discharge is significant.

Fig. 4 provides the information about spacial structure of the surface nanosecond barrier discharge in

argon/oxygen mixture. The image presented in Fig. 4 was obtained with camera gate equal to 2 ns in the middle of the pulse applied to initiate the discharge. The ratio between argon and oxygen and mixture density were chosen to correspond to the parameters in considered plasma-assisted ignition experiments. It is seen from the figure that the discharge develops as the set of streamers propagating from HV electrode to the edge of the grounded electrode. Assuming that the streamer channels have cylindrical shape and knowing from Fig. 4 the number of channels (around 120 channels) one can estimate the energy absorption per streamer and energy absorption per molecule. It should be also noticed that ICCD imaging presented in Fig. 4 was obtained in the mixture not containing hydrocarbons. It is well known that the addition of hydrocarbons can significantly change the spacial structure of the discharge. Nevertheless the fraction of hydrocarbons in combustible mixtures in considered experiments doesn't exceed four percent and we assume that the picture presented in Fig. 4 can be used as the base for the estimations.

According to the PMT measurements the sharp increase of voltage occurs at about 0.5 ms. This value can be used as the upper estimate for the actual induction time which is the combination of the induction delay time and of the period after which the wave of flame comes from the discharge to the region 1 mm apart the discharge covered by PMT. The estimations of integral absorbed energy and actual induction time give the basis for numerical modeling.

It was assumed that discharge and combustion kinetics can be considered as two relatively independent problems since the characteristic discharge time is nanoseconds and characteristic combustion chemistry time at considered conditions is at least microseconds. Finally kinetic problems were considered consequently: first - discharge kinetics, second - combustion problem with initial conditions corresponding to the output parameters of discharge kinetic problem.

The combustion kinetic mechanism used for a modeling was C3.<sup>4</sup> This mechanism was perfectly validated for the mixtures considered in this work in wide range of pressures and temperatures. The solver of differential equations ChemKin<sup>5</sup> was used for the solution of combustion kinetic problem.

The modeling was made in three steps with consequent increase of factors taken into account:

- 1) Approach A: Modeling was performed for butane/oxygen stoichiometric mixture diluted by 76 % of Ar. The discharge action was taking into account by only addition of atomic oxygen into initial conditions for combustion kinetics problem, i.e. discharge action on ignition process was considered only as dissociation of molecular oxygen.
- 2) Approach B: Modeling was performed for methane/oxygen stoichiometric mixture diluted by 76 % of Ar. The discharge action was considered as the atomic oxygen production like in approach A and also as the heating of the gas in the discharge.
- 3) Approach C: Modeling was performed for methane/oxygen stoichiometric mixture diluted by 76 % of Ar. The discharge action was considered as the production of five different active species and fast gas heating due to quenching and dissociation reactions was taking into account.

## V. Approach A: partial O<sub>2</sub> dissociation.

The preliminary modeling of plasma assisted ignition was performed in suggestion that the discharge action can be taken into account by addition of certain amount of atomic oxygen into initial conditions for combustion problem. I.e. it was assumed that the whole discharge deposited energy is distributed to the dissociation of molecular oxygen, but not to the gas heating or production of other active species. This model is significantly simplified but allows to estimate certain trends for dependencies of pressure and induction delay time.

Fig. 5 and 6 demonstrate the results of the modeling for butane/oxygen stoichiometric mixture diluted by 76 % of argon. The dependencies of pressure and OH fraction *vs* time are presented in Fig. 5 for different percentage of dissociated oxygen. It is seen from Fig. 5 that at considered conditions the discharge action can significantly change pressure and chemistry on the scale of microseconds. It should be noted that the autoignition time at considered conditions is milliseconds. At the same time Fig. 6 demonstrate non-linear dependence of the induction time *vs* percentage of the dissociated oxygen. Decrease of the induction time is more significant at lower level of dissociated oxygen, i.e. at lower discharge deposited energy. That gives an idea about the optimal spatial distribution of the energy deposited in discharge per molecule if to consider the discharge as the application for plasma-assisted combustion. The rise of pressure in the combustion chamber is caused by the process of flame propagation from the discharge to the chamber.

At considered conditions the efficient induction time is limited due to flame propagation speed. Therefore

the decrease of the actual induction time will not change significantly the efficient induction time.

At considered conditions flame propagation characteristic time is milliseconds. According to the results presented in Fig. 6 actual induction time will be shorter than efficient induction time if more than one percent of oxygen is dissociated, i.e. if the deposited energy per molecule is high enough to dissociate 1 % of oxygen. Energy deposition per molecule strongly depends on the geometry of the electrode system used to initiate the discharge. The highest deposited energy per molecule can be reached in pin-to-pin geometry of the electrode system. Work<sup>6</sup> describes the experimental results obtained for nanosecond discharge in pin-to-pin geometry. According to the authors of<sup>6</sup> the percentage of the dissociated oxygen reaches up to 50 %. At the same time pin-to-pin geometry provides the ignition in a point but not volumetric. There is a possible problem that the energy density necessary for ignition is reached but the minimal ignition volume may be not reached. The optimal electrode system should provide both - enough high deposited energy and enough big volume where this energy is reached.

## VI. Approach B. Partial O<sub>2</sub> dissociation and gas heating.

The next improvement of kinetic model was made by taking into account of the gas heating in discharge. It was assumed that the whole deposited energy is shared between two channels: dissociation of oxygen by electron impact and heating. The part of the energy spent to the dissociation in oxygen/argon mixture was calculated with BOLSIG+ software<sup>7</sup> and the rest was assumed to be spent to the gas heating. This improvement relatively to approach A is still significantly artificial since in reality deposited energy distributes between heating and production of many different species and the process is accompanied by chemical transformations. At the same time this approach allows to compare the importance of different factors for ignition chemistry: heating by the discharge and production of active particles in the discharge.

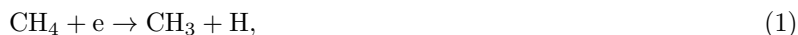
Fig. 7 demonstrates the dependence of the induction time *vs* deposited energy calculated with using of approach B. The percentage of dissociated oxygen and temperature increase due to the discharge action are signed near the point corresponding to the different deposited energies per molecule. The dependence of the induction time on the deposited energy is very strong - variation of the deposited energy two times leads to the change in induction time in 20 times.

## VII. Approach C. Kinetic scheme with different active species and fast gas heating.

In this section another more general approach to the discharge modeling for combustion problem is considered. Approach C includes the calculations of the electronic distribution function, chemical transformations and corresponding heat release during the discharge. The calculations were performed for methane/oxygen stoichiometric mixture. The cross-sections for hydrocarbon-electron reactions are known significantly better for methane than for other hydrocarbons which makes CH<sub>4</sub> content mixtures more convenient for numerical analysis of the discharge. The output results of discharge kinetic problem were used as the initial conditions for the combustion kinetic problem as it was done before.

### A. Discharge modeling

The calculations of the discharge kinetics were performed with the set of reactions presented in table 1. There is a significant production of O-atoms and CH<sub>3</sub> radicals in combustible mixture during the discharge development at considered conditions. The generation of CH<sub>3</sub> radical in the discharge is caused by two reactions:



The contribution of reaction (2) to CH<sub>3</sub> production is more significant<sup>8</sup> than the contribution of reaction (1). This partially solves the problem that the cross-section of methane dissociation by electron impact are not known perfectly.<sup>9</sup> It is necessary to note that in the discharge systems with significant concentrations of O-atoms and CH<sub>3</sub> radicals the fast transformation of O(<sup>3</sup>P) atoms into formaldehyde is possible in reaction O(<sup>3</sup>P)+CH<sub>3</sub> → CH<sub>2</sub>O+H,  $k=1.4 \cdot 10^{-10} \text{cm}^3/\text{s}$  (see<sup>10</sup>) At the same time there are the sources of fast CH<sub>3</sub>

generation:<sup>10</sup>



This means that the O(<sup>3</sup>P) atoms will disappear in the reaction with CH<sub>3</sub> whereas the CH<sub>3</sub> density will remain will be not changed rapidly. It should be noted that the reaction (5) can be accelerated due to vibrational excitation of OH molecules.

Fig. 8 demonstrates the evolutions of the active species in discharge calculated with the kinetic mechanism described above for E/N=100 Td, P=15 bar, T=940 K and deposited energy W=0.05 eV/molecule. It should be noted that the estimation of the reduced electric field in the discharge on the base of experimental data is complicated. Therefore the choice of the reduced electric field value for kinetic calculations is also difficult.

This problem can be partially solved by the taking into account the fact that G-factors are changing rather smoothly with the reduced electric field in range 80-120 Td. Fig. 9 represents the dependencies of G-factors on E/N calculated for methane/oxygen stoichiometric mixture diluted by 76 % of argon. It is seen that above E/N=80 Td the dependence of G on E/N is rather smooth. The value E/N=80 Td is definitely above the reduced electric field in the discharge at considered conditions. The reduced electric field E/N=80 Td was used for further kinetic calculations.

The gas heating mainly occurs due to the reactions of dissociation of CH<sub>4</sub> and O<sub>2</sub> molecules by electron impact and due to reactions of quenching of electronically excited O(<sup>1</sup>D) and Ar(<sup>3</sup>P<sub>0,2</sub>) atoms by O<sub>2</sub> and CH<sub>4</sub> molecules. The processes of quenching of O(<sup>1</sup>D) and Ar(<sup>3</sup>P<sub>0,2</sub>) at considered conditions are very fast and their characteristic times do not exceed 10 ns what is less than the duration of the pulse applied to initiate the discharge. That means that effective gas heating occurs during the discharge development.

Table 2 represents the results of calculations with the kinetic mechanism described above for methane/oxygen stoichiometric mixture diluted by 76 % of argon. Two cases were considered: a) when the reactions including O(<sup>1</sup>D) were involved into kinetic scheme b) when these reaction were not included. Table 2 contents the molar fractions of different active species corresponding to the instance of t=10 ns, i.e. to the middle of the pulse applied to initiate the discharge. It is seen that the increase of the temperature is higher in case when the reactions with O(<sup>1</sup>D) are not taking into account. At the same time in case when the reactions with O(<sup>1</sup>D) are included into kinetic scheme more energy is distributed into active species production. The results of calculations presented in table 2 were used as the initial conditions for further solution of combustion problem.

Table 1: System of reactions involving charged and electronically-excited particles in CH<sub>4</sub> : O<sub>2</sub> : Ar mixture

No	Reaction	Rate constant*	$\varepsilon_k$ , eV	Ref
R1	$e + \text{Ar} \rightarrow \text{Ar}^+ + 2 \cdot e$	$k = k(E/N)$		8
R2	$e + \text{O}_2 \rightarrow \text{O}_2^+ + 2 \cdot e$	$k = k(E/N)$		8
R3	$e + \text{CH}_4 \rightarrow \text{CH}_4^+ + 2 \cdot e$	$k = k(E/N)$		9
R4	$\text{Ar}^+ + \text{O}_2 \rightarrow \text{Ar} + \text{O}_2^+$	$1.0 \cdot 10^{-10}$	3.2	10
R5	$\text{Ar}^+ + \text{CH}_4 \rightarrow \text{Ar} + \text{CH}_3^+ + \text{H}$	$6.5 \cdot 10^{-10}$		10
R6	$\text{Ar}^+ + \text{CH}_4 \rightarrow \text{Ar} + \text{CH}_2^+ + \text{H}_2$	$1.4 \cdot 10^{-10}$		10
R7	$\text{CH}_4^+ + \text{O}_2 \rightarrow \text{CH}_4 + \text{O}_2^+$	$5.0 \cdot 10^{-10}$	0.5	10
R8	$\text{O}_2^+ + e \rightarrow \text{O}({}^3\text{P}) + \text{O}({}^1\text{D})$	$2.0 \cdot 10^{-7} \cdot (300/T_e)^{0.7}$	5.0	11
R9	$\text{CH}_4^+ + e \rightarrow \text{CH}_3(\nu) + \text{H} + e$	$1.7 \cdot 10^{-7} \cdot (300/T_e)^{0.5}$	8.5	10
R10	$\text{CH}_4^+ + e \rightarrow \text{CH}_2(\nu) + 2 \cdot \text{H} + e$	$1.7 \cdot 10^{-7} \cdot (300/T_e)^{0.5}$		10
R11	$\text{CH}_3^+ + e \rightarrow \text{CH}_2(\nu) + \text{H} + e$	$3.5 \cdot 10^{-7} \cdot (300/T_e)^{0.5}$		10
R12	$\text{CH}_2^+ + e \rightarrow \text{CH}(\nu) + \text{H} + e$	$2.5 \cdot 10^{-7} \cdot (300/T_e)^{0.5}$		10
R13	$e + \text{CH}_4 \rightarrow e + \text{CH}_3(\nu) + \text{H}$	$k = k(E/N)$	3.4	9
R14	$e + \text{Ar} \rightarrow e + \text{Ar}^*$	$k = k(E/N)$		8
R15	$\text{Ar}^* + \text{O}_2 \rightarrow \text{Ar} + \text{O}({}^3\text{P}) + \text{O}({}^1\text{D})^{(1)}$	$2.0 \cdot 10^{-10}$	5.4	10, 12
R16	$\text{Ar}^* + \text{CH}_4 \rightarrow \text{Ar} + \text{CH}_2(\nu) + 2 \cdot \text{H}$	$3.3 \cdot 10^{-10}$	2.3	10, 13
R17	$\text{Ar}^* + \text{CH}_4 \rightarrow \text{Ar} + \text{CH} + \text{H}_2 + \text{H}$	$5.8 \cdot 10^{-11}$	2.4	10, 13
R18	$\text{Ar}^* + \text{CH}_4 \rightarrow \text{Ar} + \text{CH}_2(\nu) + \text{H}_2$	$5.8 \cdot 10^{-11}$	6.8	10, 13
R19	$\text{Ar}^* + \text{CH}_4 \rightarrow \text{Ar} + \text{CH}_3(\nu) + \text{H}$	$5.8 \cdot 10^{-11}$	7.1	10, 13
R20	$e + \text{O}_2 \rightarrow e + \text{O}({}^3\text{P}) + \text{O}({}^3\text{P})^{(2)}$	$k = k(E/N)$	1.0	14, 15
R21	$e + \text{O}_2 \rightarrow e + \text{O}({}^3\text{P}) + \text{O}({}^1\text{D})^{(2)}$	$k = k(E/N)$	1.0	14, 15

Table 1: System of reactions involving charged and electronically-excited particles in CH<sub>4</sub> : O<sub>2</sub> : Ar mixture

No	Reaction	Rate constant*	$\epsilon_k$ , eV	Ref
R22	$O(^1D) + O_2 \rightarrow O(^3P) + O_2(b^1\Sigma_g, \nu)$	$3.2 \cdot 10^{-11} \cdot \exp(67/T)$	0.34	16
R23	$O(^1D) + CH_4 \rightarrow CH_3 + OH^{(3,4)}$	$2.2 \cdot 10^{-10}$	1.86	17
R24	$O(^1D) + Ar \rightarrow O(^3P) + Ar$	$7.7 \cdot 10^{-13}$	1.97	18
R25	$e + O_2 \rightarrow e + O_2(A,c,C)$	$k = k(E/N)$		14, 15
R26	$e + O_2 \rightarrow e + O_2(b^1\Sigma_g)$	$k = k(E/N)$		14, 15
R27	$e + O_2 \rightarrow e + O_2(a^1\Delta_g)$	$k = k(E/N)$		14, 15
R28	$O_2(A) + O(^3P) \rightarrow O_2(b^1\Sigma_g) + O(^3P)$	$0.9 \cdot 10^{-11}$	2.54	16
R29	$O_2(A) + O_2 \rightarrow O_2 + O_2(b^1\Sigma_g, \nu)$	$2.9 \cdot 10^{-13}$	2.8	16
R30	$O_2(A) + CH_4 \rightarrow CH_4(\nu) + O_2(b^1\Sigma_g)$	$> 1.0 \cdot 10^{-12}$ (estimation)	2.8	<i>p.w.</i>
R31	$O_2(b^1\Sigma_g) + O_2 \rightarrow O_2(a^1\Delta_g) + O_2(\nu)^{(5)}$	$4.0 \cdot 10^{-17}$	0.65	19
R32	$O_2(b^1\Sigma_g) + CH_4 \rightarrow O_2(a^1\Delta_g) + CH_4(\nu)^{(5)}$	$(7-10) \cdot 10^{-14}$	0.65	19
R33	$O_2(a^1\Delta_g) + O_2 \rightarrow O_2(\nu) + O_2(\nu)$	$2.0 \cdot 10^{-18}$	0.98	19
R34	$O_2(a^1\Delta_g) + CH_4 \rightarrow O_2 + CH_4(\nu)$	$1.4 \cdot 10^{-18}$	0.98	19
R35	$O_2(a^1\Delta_g) + HO_2 \rightarrow O_2 + HO_2^*$	$2.0 \cdot 10^{-11}$	0.98	22
R36	$O_2(a^1\Delta_g) + H \rightarrow O(^3P) + OH$	$1.3 \cdot 10^{-11} \cdot \exp(-2530/T)$		22
R37	$O_2(a^1\Delta_g) + H \rightarrow O_2 + H$	$5.2 \cdot 10^{-11} \cdot \exp(-2530/T)$	0.98	22
R38	$O_2(\nu = 1) + O(^3P) \rightarrow O_2(\nu = 0) + O(^3P)$	$1.2 \cdot 10^{-12} \cdot (T/300)$		23
R39	$O_2(\nu) + CH_4 \rightarrow O_2(\nu = 0) + CH_4(\nu)^{(6)}$	$k_{\nu\nu'}(T)$		24
R40	$CH_4(\nu) + CH_4 \rightarrow CH_4(\nu = 0) + CH_4^{(7)}$	$k_{\nu T}(T)$		25-27

\* Dimensions for two-body reactions is cm<sup>3</sup>/s; dimensions for tree-body reactions is cm<sup>6</sup>/s.

Table 2: Production of active species in CH<sub>4</sub>:O<sub>2</sub>:Ar=8:16:76 mixture. P=15 bar, T=960 K, E/N=80 Td, W=0.07

	O <sup>(3)P</sup> /N	H/N	OH/N	CH <sub>3</sub> /N	CH <sub>2</sub> /N	O <sub>2</sub> (b)	$\delta T$ , K
with O <sup>(1)D</sup>	$7.15 \cdot 10^{-3}$	$1.74 \cdot 10^{-3}$	$3.47 \cdot 10^{-3}$	$4.73 \cdot 10^{-3}$	$2.41 \cdot 10^{-4}$	$4.28 \cdot 10^{-3}$	58
without O <sup>(1)D</sup>	$1.06 \cdot 10^{-2}$	$1.75 \cdot 10^{-3}$	0	$1.27 \cdot 10^{-3}$	$2.42 \cdot 10^{-4}$	$3.21 \cdot 10^{-3}$	64

## B. Results with Approach C

The calculations with Approach C were performed for methane stoichiometric mixture at P=15 bar and in temperature range T=400-960 K. The concentrations of active species generated in discharge and temperature increase due to fast gas heating were calculated with the kinetic scheme described in previous subsection. Then these parameters were used as the initial conditions for combustion kinetic problem.

Fig. 10-12 demonstrate the results obtained with Approach C. Fig. 10 demonstrates the importance of the inclusion into discharge kinetic scheme of reactions with O<sup>(1)D</sup>. Solid line in Fig. 10a represents the case when the reactions with O<sup>(1)D</sup> were included into discharge kinetic scheme and dashed line when the reactions with O<sup>(1)D</sup> were not included. The difference in combustion kinetics for "with" O<sup>(1)D</sup> and "without" O<sup>(1)D</sup> cases demonstrates the importance of reactions with O<sup>(1)D</sup> in the discharge kinetic scheme. The dependencies of temperature for "with" O<sup>(1)D</sup> and "without" O<sup>(1)D</sup> cases are presented in Fig. 10b. It is seen that even despite lower temperature increase due to fast gas heating in "with" O<sup>(1)D</sup> case (see table 2) the temperature takes higher values in this case due to higher concentrations of active species in the discharge. This is another demonstration of necessity to include the reactions with O<sup>(1)D</sup> into discharge kinetic scheme.

Fig. 11 represents the dependence of the induction time *vs* initial gas temperature for three cases: a) when the reactions with O<sup>(1)D</sup> were included into discharge kinetic scheme b) when the reactions with O<sup>(1)D</sup> were not included c) when it was assumed that the whole deposited energy was distributed to the gas heating. Case c) is equivalent to the autoignition case at higher initial gas temperatures. Fig. 11 shows that the reactions with O<sup>(1)D</sup> are important at lower temperatures. This figure also demonstrates that at the same discharge deposited energy the decrease of the induction time is occurs more due to active species production than to the heating. This allows to ignite, with the same amount of energy, the mixture which cannot be ignited by only heating.

Fig. 12 represents the kinetic curves for different species for 400 K and 960 K. These temperatures were

chosen as the limiting cases in the investigated range of parameters. Fig. 12 demonstrates that at the considered conditions after approximately 1  $\mu$ s the chemical reforming due to generated by discharge active species is complete and species concentrations reach the stationary level.

## VIII. Conclusions

Numerical study of the parameters of plasma-assisted ignition has been performed for methane/oxygen stoichiometric mixture diluted by 76 % of Ar at P=15 bar and T=400-960 K. The dependence of the induction time *vs* discharge deposited energy per molecule was calculated and appeared very sharp. The energy necessary for significant decrease of the induction time was found relatively low. That demonstrates the advantage for ignition application of the discharge with spatially distributed and relatively low deposited energy per molecule before the discharge with high energy per molecule but released in the point. The synergetic effect due to production of active species and increase of the temperature due to fast gas heating leads to efficient ignition of combustible mixtures even at conditions when autoignition is not possible. The kinetic curves for main active species in early discharge afterglow were calculated. The importance of the reactions with O(<sup>1</sup>D) in discharge kinetic scheme at lower temperatures was demonstrated. According to the calculations, the chemical reforming due to the active species produced by discharge is complete in 500  $\mu$ s at considered conditions.

## Acknowledgements

The authors are thankful to Prof. Yu. Akishev (TRINITI) and Dr. M. Shneider (Princeton University) for helpful discussions and to J. Guillon for technical assistance. The work was partially supported by French National Agency, ANR (PLASMAFLAME Project, 2011 BS09 025 01), PICS-RFBR grant (5745-11.02.91063-a/5745), AOARD AFOSR, FA2386-13-1-4064 grant, RFBR project 10-01-00468-a, and by PUF (Partner University Foundation).

## References

- <sup>1</sup>Kosarev I, Khorunzhenko V, Mintousov E, Sagulenko P, Popov N and Starikovskaia S, 2012 A nanosecond surface dielectric barrier discharge at elevated pressures: time-resolved electric field and efficiency of initiation of combustion. *Plasma Sources Sci. Technol.* **20** 045002
- <sup>2</sup>Stepanyan S, Vanhove G, Desgroux P and Starikovskaia S, 2013 Time-resolved electric field measurements in nanosecond surface dielectric discharge. Comparison of different polarities. Ignition of combustible mixtures by surface discharge in a rapid compression machine. *AIAA Meeting (Grapevine, Texas, January 2013)* AIAA 2013-1053
- <sup>3</sup>Boumejdi M, Stepanyan S, Starikovskaia S, Desgroux D, Vanhove G., 2013 Plasma assisted ignition inside a Rapid Compression Machine. Proceedings of European Combustion meeting.
- <sup>4</sup>Healy D, Kalitan D, Aul C, Petersen E, Bourque G and Curran H, 2010 Oxidation of C1-C5 Alkane Quinary Natural Gas Mixtures at High Pressures. *Energy Fuels* **24** 1521-1528
- <sup>5</sup>Kee R *et al*, 2000 CHEMKIN Collection, Release 3.6, Reaction Design, Inc., San Diego, CA
- <sup>6</sup>Rusterholtz D, Lacoste D, Stancu G, Pai D and Laux C, 2013 Ultrafast heating and oxygen dissociation in atmospheric pressure air by nanosecond repetitively pulsed discharges. *Journal of Physics D* **46** 464010
- <sup>7</sup>Hagelaar G and Pitchford L, 2005 Solving the Boltzmann equation to obtain electron transport coefficients and rate coefficients for fluid models. *Plasma Sources Sci. Technol.* **14** 722-733
- <sup>8</sup>Hayashi M, 1987 Electron collision cross sections for molecules determined from beam and swarm data *Pitchford L.C., McCoy B.V., Chutjian A., Trajmar S. (Eds.), Swarm studies and inelastic electron-molecule collisions, Springer-Verlag, New York* 167-187
- <sup>9</sup>Morgan W L, 1992 A critical evaluation of low-energy electron impact cross sections for plasma processing modeling. *Plasma Chemistry and Plasma Processing* **12** 477
- <sup>10</sup>Kosarev I N, Aleksandrov N L, Kindysheva S V, Starikovskaia S M, Starikovskii A Yu, 2008 Kinetics of ignition of saturated hydrocarbons by nonequilibrium plasma: CH<sub>4</sub>-containing mixtures. *Combustion and Flame* **154** 569-586
- <sup>11</sup>Florescu-Mitchell A I, Mitchell J B A, 2006 Dissociative recombination. *Physics Reports* **430** 277- 374
- <sup>12</sup>Balamuta J, Golde M F 1982 Formation of electronically excited oxygen atoms in the reactions of Ar(<sup>3</sup>P<sub>0,2</sub>) and Xe(<sup>3</sup>P<sub>2</sub>) atoms with O<sub>2</sub>. *J. Phys. Chem.* **86** 2765
- <sup>13</sup>Balamuta J, Golde M F, Ho Y, 1983 Product distributions in the reactions of excited noble gas atoms with hydrogen-containing compounds. *J. Chem. Phys.* **79** 2822
- <sup>14</sup>Braginsky O V, Vasilieva A N, Klopovskiy K S, Kovalev A S, Lopaev D V, Proshina O V, Rakhimova T V, Rakhimov A T 2005 Singlet oxygen generation in O<sub>2</sub> flow excited by RF discharge. *J. Phys. D: Appl. Phys.* **38** 3609-3625

- <sup>15</sup>Kovalev A S, Lopaev D V, Mankelevich Yu A, Popov N A, Rakhimova T V, Poroykov A Yu, Carroll D L 2005 Kinetics of  $O_2(b^1\Sigma_g)$  in oxygen RF discharges. *J. Phys. D: Appl. Phys.* **38** 2360-2370
- <sup>16</sup>Kossyi I A, Kostinsky A Y, Matveev A A, Silakov V P 1992 Kinetic scheme of the non-equilibrium discharge in nitrogen-oxygen mixtures. *Plasma Sources Sci. Technol.* **1 N 3** 207-220
- <sup>17</sup>Vranckx S, Peeters J, Carl S 2008 A temperature dependence kinetic study of  $O(^1D) + CH_4$ : overall rate coefficient and product yields. *Phys. Chem. Chem. Phys.* **10** 5714-5722
- <sup>18</sup>Kinnersly S R, Murrell J N, Rodwell W R Collisional Quenching of  $O(^1D)$  by rare gas atoms
- <sup>19</sup>Morozov I I, Temchin S M 1989 Kinetics of the reaction of singlet oxygen in the gas phase *Plasma Chemistry M. Energoatomizdat.* **16** 39-67
- <sup>20</sup>Dvoryankin A N, Ibragimov L B, Kulagin Y A, Shelepin L A 1987 Mechanisms of electron relaxation in atomic and molecular systems. *Plasma Chemistry. Moscow: Energoatomizdat.* **14** 102-127
- <sup>21</sup>Radzig A A, Smirnov B M 1980 Reference data on atoms, molecules and ions. (*Berlin, Springer*)
- <sup>22</sup>Popov N A 2011 Effect of singlet oxygen  $O_2(a^1\Delta_g)$  molecules produced in gas discharge plasma on the ignition of hydrogen-oxygen mixtures. *Plasma Sources Sci. Technol.* **20** 045002
- <sup>23</sup>McEwan M J, Phillips L F 1975 Chemistry of the Atmosphere, *Edward Arnold*
- <sup>24</sup>White D R 1965 Vibrational relaxation of oxygen by methane, acetylene, and ethylene. *J. Chem. Phys.* **42** 2028-2032
- <sup>25</sup>Stretton J L 1965 Calculation of vibrational relaxation times in polyatomic gases. *Trans. Faraday Soc.* **61** 1053-67
- <sup>26</sup>Perrin M Y, Jolicard G 1986 Rovibrational energy transfer in mixtures of  $CH_4$  and  $CD_4$  with He and Ne. *Chem. Phys. Lett.* **127 No 2** 118
- <sup>27</sup>Richards L W, Sigafos D H 1965 Vibrational relaxation of methane. *J. Chem. Phys.* **43** 492
- <sup>28</sup>Popov N A 2010 Evolution of the negative ion composition in the afterglow of a streamer discharge in air. *Plasma Physics Reports.* **36** 812-818
- <sup>29</sup>Matsumi Y, Tnokura K, Inagaki Y and Kawasaki M Isotopic branching ratios and translational energy release of H and D atoms in reaction of  $O(^1D)$  atoms with alkanes and alkyl chlorides. *J. Phys. Chem.* **97** 6816-6821
- <sup>30</sup>Capitelli M, Ferreira C M, Gordiets B F, Osipov A I 2000 Plasma kinetics in atmospheric gases. *Springer* 297
- <sup>31</sup>Aleksandrov N L, Kindusheva S V, Nudnova M M, Starikovskii A Yu 2010 Mechanism of ultra-fast heating in a non-equilibrium weakly ionized air discharge plasma in high electric fields. *J. Phys. D: Appl. Phys.* **43** 255201 (19 pp)
- <sup>32</sup>Doroshenko V M, Kudryavtsev N N, Smetanin V V 1992 Mechanisms of quenching of electronically excited particles in a partially dissociated air. *HVE* **26** 291
- <sup>33</sup>Kosarev I N, Aleksandrov N L, Kindysheva S V, Starikovskaia S M, Starikovskii A Yu 2009 Kinetics of ignition of saturated hydrocarbons by nonequilibrium plasma:  $C_2H_6$  - to  $C_5H_{12}$  - containing mixtures. *Combustion and Flame* **156** 221-233
- <sup>34</sup>Holmes R, Jones G R, Pusat N 1964 Vibrational relaxation in propane, propylene and ethane. *J. Chem. Phys.* **41** 2512-2516
- <sup>35</sup>Magne L, Pasquiers S, Gadonna K, Jeanney P, Blin-Simiand N, Jorand F and Postel C 2009 OH kinetic in high-pressure plasmas of atmospheric gases containing  $C_2H_6$  studied by absolute measurement of the radical density in a pulsed homogeneous discharge. *J. Phys. D: Appl. Phys.* **42** 165203 (17pp)

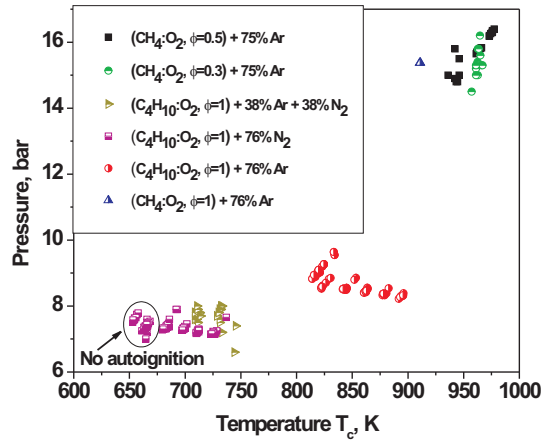


Figure 1. The range of parameters investigated in plasma-assisted experiments.

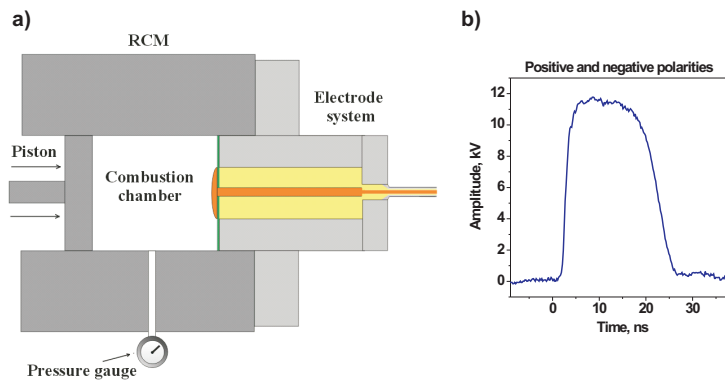


Figure 2. a) scheme of combustion chamber of rapid compression machine with mounted discharge electrode system. b) pulses applied to initiate the discharge

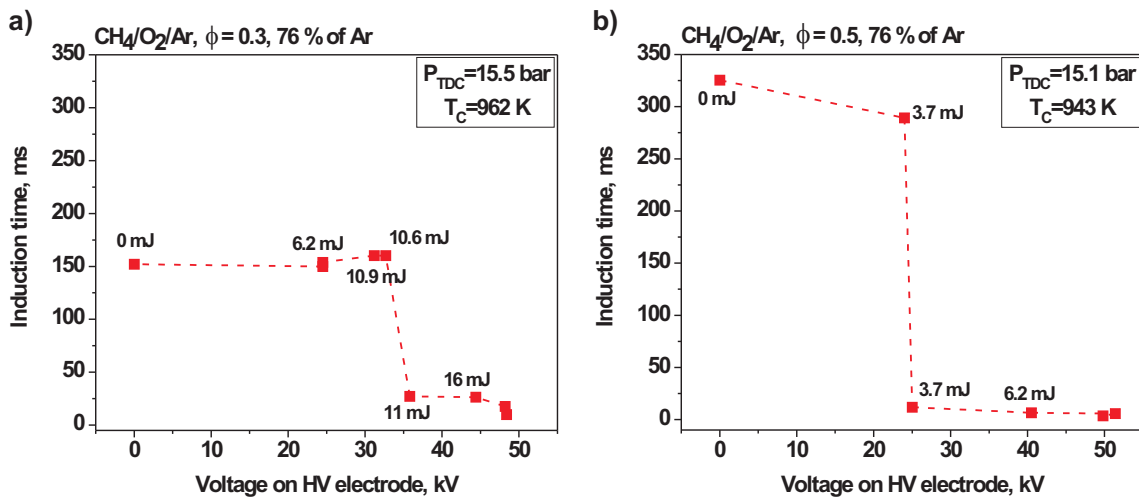


Figure 3. Dependence of the induction time *vs* applied voltage for different equivalence ratio. Methane/oxygen mixtures diluted by 76 % of argon. Numbers above experimental points note the discharge deposited energy.

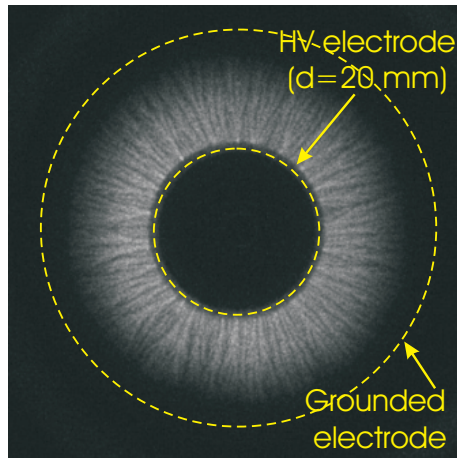


Figure 4. Characteristic ICCD image of the discharge in argon/oxygen=3.7/1 mixture. Pressure is 3.2 bar. Camera gate is 2 ns.

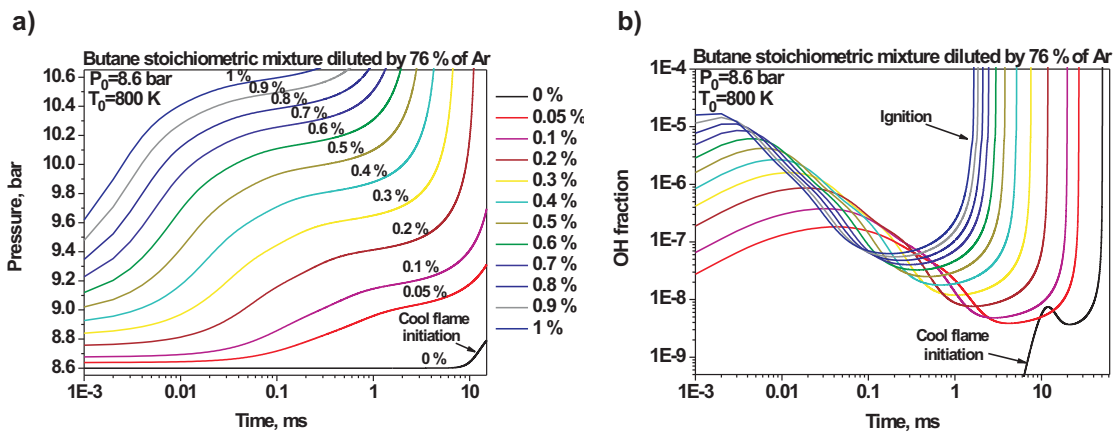


Figure 5. Butane stoichiometric mixture diluted by 76 % of argon,  $T=800$  K,  $P=8.6$  bar. a) dependence of the pressure vs time b) dependence of OH fraction vs time. Numbers near the curves note the percentage of  $O_2$  dissociated due to discharge action.

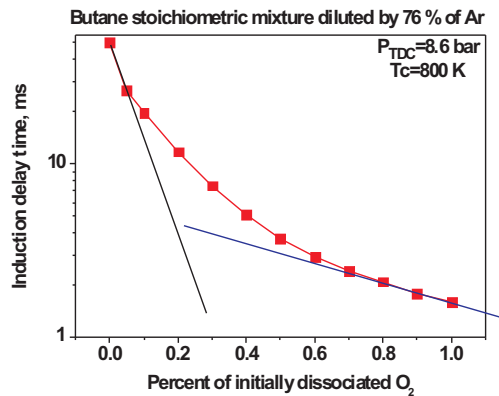


Figure 6. Dependence of the induction time vs percentage of dissociated oxygen,  $T=800$  K,  $P=8.6$  bar. Butane stoichiometric mixture diluted by 76 % of argon.

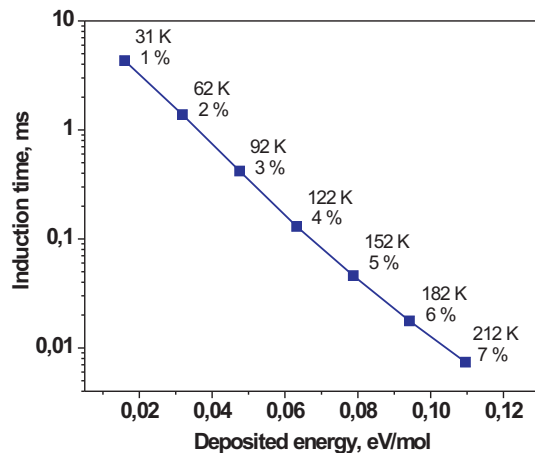


Figure 7. Dependence of the induction time *vs* percentage of dissociated oxygen,  $T=960$  K,  $P=16$  bar. Methane stoichiometric mixture diluted by 76 % of argon.

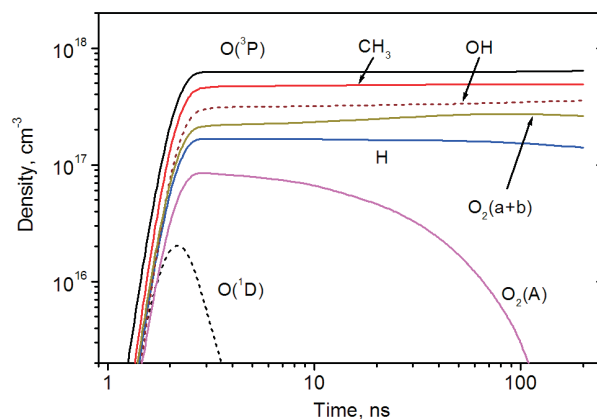


Figure 8. The evolution of active species fractions calculated at  $E/N=100$  Td for methane/oxygen stoichiometric mixture diluted by 76.  $P=15$  bar,  $T=940$  K, deposited energy  $W=0.05$  eV/molecule

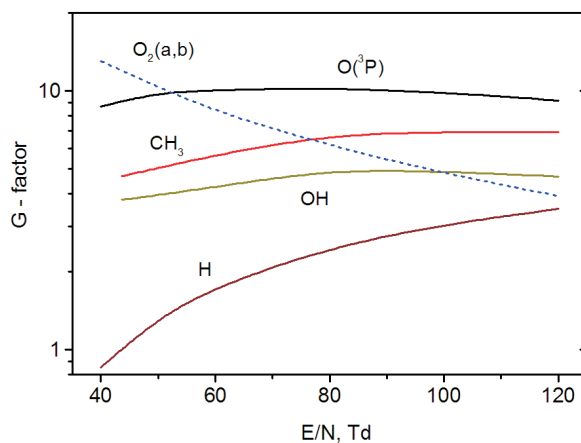


Figure 9. G - factors *vs* E/N calculated for methane/oxygen stoichiometric mixture diluted by 76 % of argon.  $P=15$  bar,  $T=940$  K.

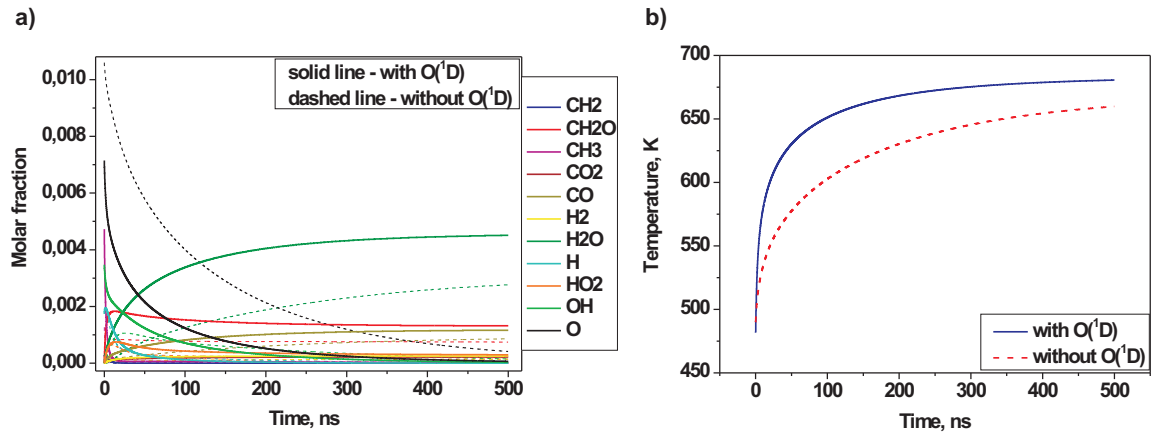


Figure 10. Comparison of kinetic models including and not including the reaction with  $O(^1D)$ . Methane stoichiometric mixture diluted by 76 % of argon,  $T=400$  K,  $P=15$  bar. a) The dependence of the fraction of active species *vs* time. Solid line - with  $O(^1D)$ , dashed - without  $O(^1D)$ . b) Dependence of temperature *vs* time. Solid line - with  $O(^1D)$ , dashed - without  $O(^1D)$

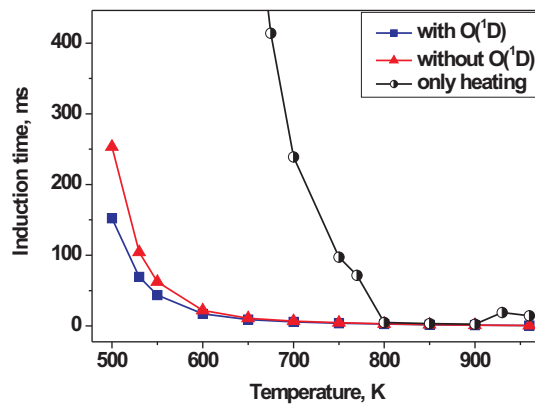


Figure 11. Dependencies of the induction time *vs* initial gas temperature. Methane stoichiometric mixture diluted by 76 % of argon,  $P=15$  bar. Squares - reactions with  $O(^1D)$  are included, triangles - reactions with  $O(^1D)$  are not included, circles - all the deposited energy distributed to the heating with no active species production.

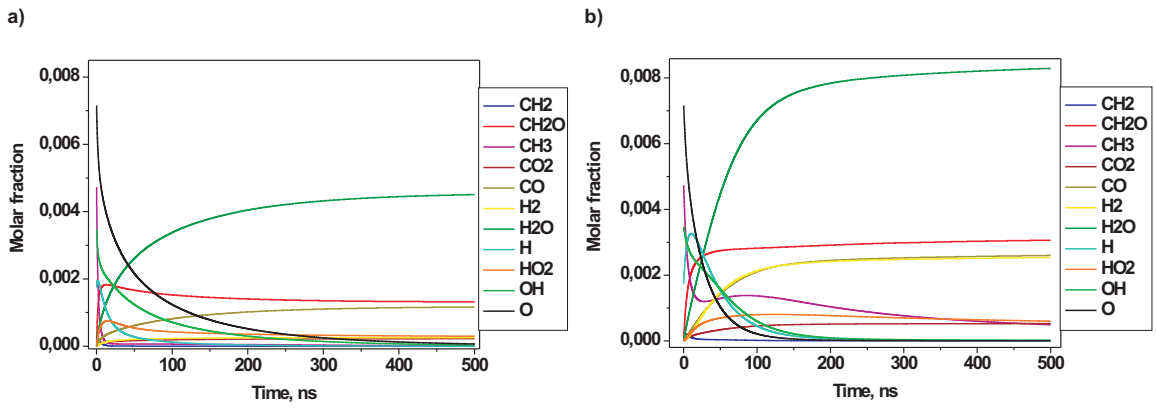


Figure 12. Fractions of active species *vs* time for a)  $T=400\text{ K}$ ,  $P=15\text{ bar}$  and b)  $T=960\text{ K}$ ,  $P=15\text{ bar}$ . Methane stoichiometric mixture diluted by 76 % of argon.